



OPEN Lateral spreading mitigation in gravity quay walls backfilled with coral sand through electrolysis desaturation treatment

Junwei Guo¹, Yumin Chen^{1,2}✉, Xiao Xie¹, Yingkang Yao³, Changchun Li⁴ & Qiongtong Wang¹

Quay walls constructed on hydraulically filled coral sand deposits face inevitable liquefaction-induced hazards during seismic events. For mitigation, electrolysis method can be employed as an induced partial saturation technique to improve the liquefaction resistance of these coral sand foundations. This study performed two blast-induced liquefaction tests on a gravity quay wall founded on coral sand, comparing the structure's response under fully saturated conditions versus desaturated condition. The primary objectives are to investigate the seismic behavior of gravity quay walls during earthquakes and to evaluate the mechanical response of sandy soils under lateral spreading in hydraulically filled coral sand deposits. Using blast-induced liquefaction, this study examines the effects of lateral spreading on gravity quay walls, revealing that the seismic acceleration response at the base is significantly amplified. The research results indicate that when saturation is reduced by 18.8%, the liquefaction duration is reduced by 30–50%, the pore water pressure ratio is reduced by 40%, the soil liquefaction resistance is strengthened, and the damage level of the gravity quay wall is reduced from Level III to Level II. The desaturation method has a certain effect on treating lateral spread of liquefaction and reducing the degree of damage to quay walls.

Keywords Coral sand, Electrolysis desaturation, Blast-induced liquefaction, Gravity quay wall

Coral sand is widely distributed in tropical and subtropical shallow marine areas between the Tropics of Cancer and Capricorn, especially abundant in the Indian Ocean-Pacific region, accounting for 91.9% of the world's total coral reef area. Countries in these regions possess abundant coastal resources, and 90% of international trade relies on maritime transport. Therefore, these countries may need to establish ports in areas where coral sand constitutes the shoreline. However, as an ocean engineering backfill material, coral sand exhibits significantly different liquefaction characteristics compared to onshore sand. Due to its unique porous structure and biological debris content, the high friability of coral sand particles causes density to be difficult to maintain stably during backfilling. This greatly increases the risk of liquefaction, leading to port damage.

Gravity quay wall is a common type of port structure that maintain stability through the weight of the caissons themselves and internal fill material. Typically, both the internal fill material and the fill behind the walls are made from in-situ materials. When coral sand is used as the hydraulic filling material, its porous, nonhomogeneous, and discontinuous nature leads to significant challenges. The filling process deposits loose coral particles, forming island reefs with near-saturation water content. As a result, these newly formed deposits exhibit extreme susceptibility to liquefaction¹. For example, during the 1993 Guam earthquake², the 1995 Hanshin Earthquake³ in Japan, the 2006 Hawaii earthquake⁴, and the 2010 Haiti earthquake, lateral spreading caused by liquefaction led to damage to embankments and ports, paralyzing the transport functions of the islands and resulting in significant economic losses. Damage caused by lateral spreading due to liquefaction has also been reported in previous studies^{5–8}.

Through shaking table tests on slopes with different gradients, Zhang⁹ found that both increasing slope gradients and seismic intensity would increase lateral flow distances. The results demonstrate that lateral spreading potential increases with greater gravity potential energy. Harbors constructed with hydraulic fill in

¹State Key Laboratory of Precision Blasting, Hohai University, Nanjing 210024, China. ²School of Civil Engineering, Suzhou University of Science and Technology, Suzhou 215011, China. ³State Key Laboratory of Precision Blasting, Jiangnan University, Wuhan 430056, China. ⁴Yellow River Conservancy Commission Henan River Affairs Bureau, Zhengzhou 450003, China. ✉email: ymch@hhu.edu.cn

deepwater environments face particularly severe risks of lateral spreading due to these conditions. Therefore, the movement of gravity quay walls during site liquefaction in earthquakes has drawn significant attention. Some researchers^{10–12} have combined case studies of port structure deformation during earthquakes with shake table tests to explain the lateral displacement damage mechanisms of gravity quay walls and evaluate their seismic performance. Their research has further examined the impacts of foundation characteristics and backfill material properties on gravity quay wall displacement patterns and adjacent pore water pressure distribution. However, these studies focused solely on the liquefaction dynamics of gravity quay walls themselves, without examining mitigation strategies for liquefaction-induced damage.

Therefore, this study investigates liquefaction mitigation methods for gravity quay walls in hydraulic fill soils. The traditional techniques include static drainage consolidation (e.g., vacuum preloading^{13–17} and surcharge preloading^{18–20}), dynamic drainage consolidation (e.g., dynamic compaction^{21–23}), and pile foundation methods (e.g., compacted sand pile^{24–28} and vibroflotation gravel piles^{29,30}). While these traditional methods offer operational convenience and controllable work processes, their requirement for multiple interconnected devices results in high costs. This highlights the need to develop more economical liquefaction mitigation techniques for hydraulic fills.

The desaturation method represents a novel liquefaction mitigation technique that differs fundamentally from traditional approaches. Desaturation methods can be classified according to the method of gas generation into air injection, microbial-induced desaturation, chemical desaturation, and electrolytic desaturation. Air injection, microbial-induced desaturation^{31–33}, and chemical desaturation require overcoming the injection pressure to introduce gas, bacteria with culture medium, chemical substances, and other materials into the foundation. These substances react within the foundation to produce gas. During injection, the soil's stress state is altered. After the reaction is complete, residual microbial organisms or chemical substances may cause problems for the local microbial community and pollution to the environment. However, the electrolytic desaturation method does not have this shortcoming. Electrolysis emerges as the least expensive and most eco-friendly option: it adds no solid material, preserves in-situ porosity and requires only reusable graphite-felt electrodes plus a low-voltage DC source. In hydraulic-fill or artificial-island settings the felt layers can be placed at any desired elevation during routine sand deposition, giving precise vertical control and immediate gas generation once current is applied.

Electrolytic preserve the porosity and stress state of sandy soils, this technique reduces soil saturation by replacing pore water with gas through water electrolysis. In this process, water acts as the reactant, dissociating into hydrogen and oxygen under direct current. The chemical reactions occurring between the two electrodes are as follows:

At the cathode:



At the anode:



The desaturation method offers significant advantages over traditional techniques, requiring neither large quantities of fill material nor complex equipment, while its cost-effectiveness has been well documented in previous studies^{34–36}. The effectiveness of method for liquefaction mitigation has been experimentally validated through shaking table tests, including evaluations conducted on free field condition³⁷ and under the existing buildings³⁸. The long-term efficacy of the desaturation method has been confirmed through systematic in situ monitoring^{36,39}.

Zhang⁴⁰ and Chen⁴¹ used pure water with added NaCl to simulate seawater in their investigation of bubble evolution characteristics in coral sand during electrolysis. Chen⁴¹ also evaluated the gas generation rate under different current intensities (1A, 2A, 4A), with results showing the highest gas retention at 1 A. Recently, Ren⁴² conducted electrolysis desaturation treatment on coral sand foundations under existing buildings and discussed the impact of multiple explosions on the stability of multi-story building foundations on reefs.

Few studies have examined liquefaction in loose coral sand fill behind quay walls under electrolysis desaturation treatment. This study investigates such fill behind a model quay wall, employing electrolysis desaturation as a foundation treatment. Using blast-induced liquefaction as the triggering mechanism, we analyze both lateral spreading of gravity quay walls on reclaimed foundations and liquefaction behavior of the surrounding soil.

Materials and methods

Calcareous sand

In this study, coral sand, which is widely distributed in the South China Sea, was used to prepare the models. The coral sand particles are light white in color, with rough and porous surfaces, sharp edges and irregular shapes. Classified as SM (Silty sand) according to the Unified Soil Classification System (USCS) of ASTM D 2487-93⁴³. The grain size distribution curve of coral sand is shown in Fig. 1, the basic physical parameters of coral sand are shown in Table 1.

Explosive

Customized black powder with a TNT equivalent of 0.05 kg was utilized in the experiments. Upon detonation, a substantial amount of energy was released, inducing liquefaction in the model. The chemical reaction equation during the explosion process is as follows:

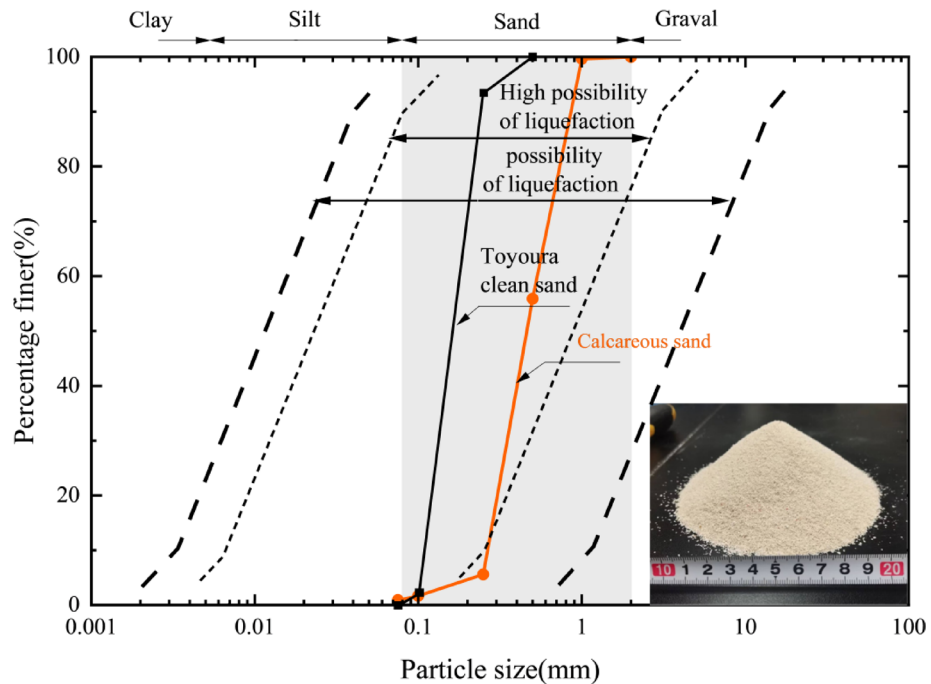
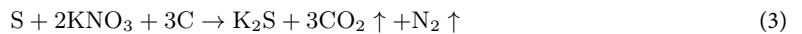


Fig. 1. Grain size distribution curve of coral sand.

Physical parameters	G_s	$\rho_{d, \max}$ (g/cm ³)	$\rho_{d, \min}$ (g/cm ³)	dD_{50} (mm)	C_c	C_u
Value	2.83	1.56	1.38	0.46	0.86	1.99

Table 1. Basic physical parameters of the coral sand.



Gravity quay wall

The gravity quay wall was made by 3D printing technology, the test model was scaled based on Dong's⁴⁴ model, which measured length \times width \times height = 2980 mm \times 1620 mm \times 2190 mm. C30 concrete and HPB335 steel bars were used as materials, where the elastic modulus of C30 concrete was 3.0×10^4 MPa. In this study, the model dimensions were length \times width \times height = 745 mm \times 405 mm \times 548 mm, and constructed from steel fiber-reinforced concrete. The model dimensions are illustrated in Fig. 2. Following laboratory testing, the elastic modulus of the material was determined to be 1.5×10^4 MPa. Therefore, the similarity ratio of the dimensions is 1:4 and the similarity ratio of elastic modulus is 1:2. Since the deformation of the quay wall is not considered in the test, this formula with an elastic modulus of 1.5×10^4 MPa was used to build the test model. The target elastic modulus was attained using a mix proportion of 1 part water, 2 parts cement, 0.83 parts coarse sand, 1 part fine sand, and 0.33 parts silica fume. Additionally, the mixture included 50 g of thickener and 30 g of fiber for every 3 kg of water to facilitate quay wall formation. Since the 3D-printed material cannot maintain unsupported overhangs, the quay wall was divided into multiple components. These were printed separately and later joined using epoxy resin after achieving sufficient strength. Figure 3 shows the process of producing the quay wall using 3D printing and the final completed quay wall model.

Field experimental program

The dimensions of the model for tests were 2.3 m \times 1.1 m \times 0.8 m, and it was surrounded by clay. Prior to model preparation, an impervious geomembrane and felt layer were first installed along the boundaries of the excavated field to create a watertight barrier and mitigate dynamic wave reflection. Subsequently, the saturated sand layer was prepared using the water sedimentation method, resulting in an overall relative density of approximately 50% for the calcareous sand foundation formation.

During the preparation of the model, the explosive packages, pore water pressure transducers, piezo accelerometers, graphite felts, and the gravity quay wall were properly arranged in the appropriate locations as shown in Fig. 4. The pore pressure transducers are located at the intersection points of each section and level. Accelerometers were fixed at the center of the back face of quay wall at three heights: top (depth = 0.15 m), mid-height (depth = 0.35 m) and bottom (depth = 0.55 m) of the substructure. These sensors measured horizontal acceleration (x-direction in Fig. 5). Electrolysis technique was used to desaturate the field in the test, and there were three layers of conductive graphite felts arranged at the corresponding locations. In addition, electrolysis

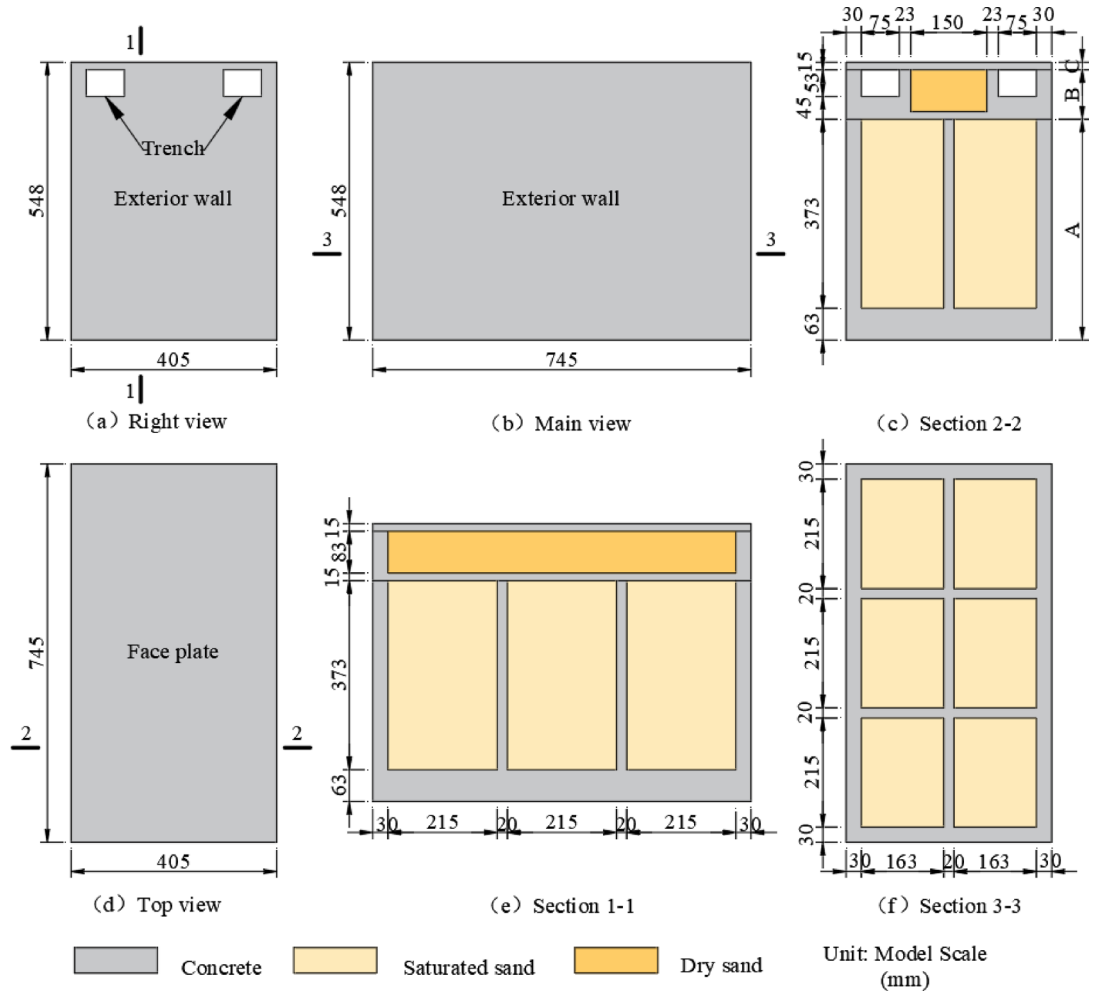


Fig. 2. Three views and sections of gravity quay wall model.

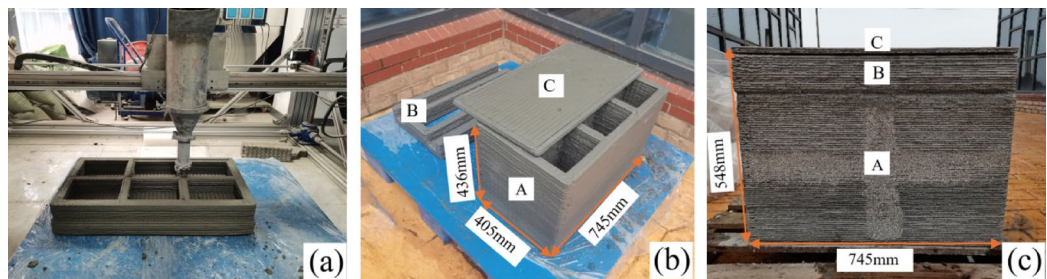


Fig. 3. Gravity quay wall fabrication process: (a) Printing the main process; (b) Quay wall components fabricated; (c) Model of the completed quay wall.

was employed to desaturate the test model. Three layers of conductive graphite felt (900 mm × 745 mm each) were installed at designated locations—two connected to the negative electrode (green line) and one to the positive electrode (red line)—to create a homogeneous, partially saturated ground layer. The final prepared test model is shown in Fig. 4 and Fig. 5.

Desaturation treatment

For the desaturation treatment, electrolysis was conducted for 4 h while maintaining a constant current of 1 A, according to Chen’s⁴¹ research, the selected current can obtain lower saturation. Explosive detonation was then performed after the equivalent resistance stabilized. The process of equivalent resistance during electrolysis is shown in Fig. 6. During the initial 20 min of electrolysis, resistivity increased rapidly by 10.4% due to bubble generation. Subsequently, as some bubbles overflowed, the rate of resistivity change gradually decreased. After 4

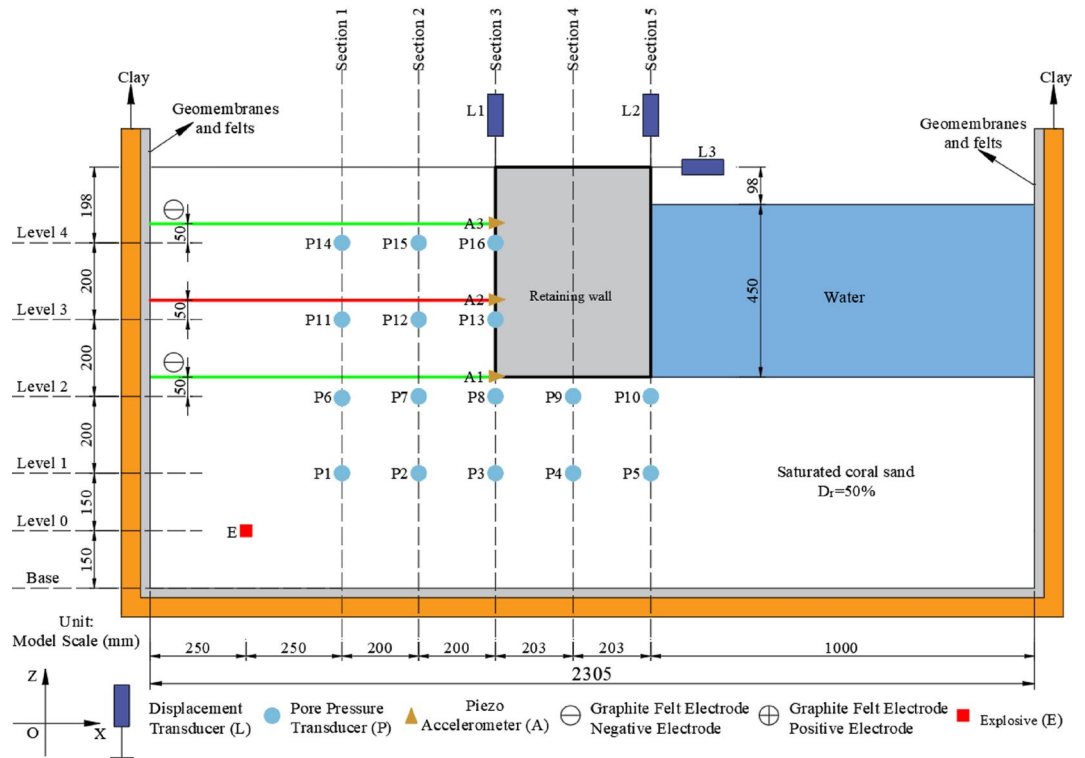


Fig. 4. Schematic of sensor and model arrangement in the experiment.

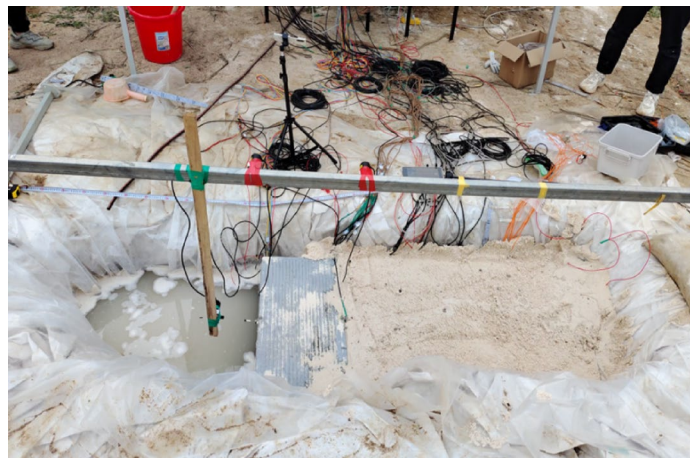


Fig. 5. Photo of completed model preparation.

h of electrolysis, the system reached a stable state with a final resistivity of 88.4 Ω·m, representing a total increase of 22%. Based on the resistivity model for unsaturated sands developed by Keller and Frischknecht⁴⁵ (Eq. 4), the saturation degree decreased from 100 to 81.2%.

$$\rho = \alpha \rho_w n^{-m} S_r^{-p} \tag{4}$$

where ρ is the resistivity of the soil; α is the saturation coefficient; ρ_w is the resistivity of the pore fluid; n is the porosity; S_r is the saturation; m is the cementation factor; and p is the saturation factor.

Experimental results and discussion

Acceleration response

To analyze the acceleration of the gravity quay wall at different saturation degrees, three acceleration sensors were fixed at different depths in the back of the quay wall. The time history of acceleration at different depths

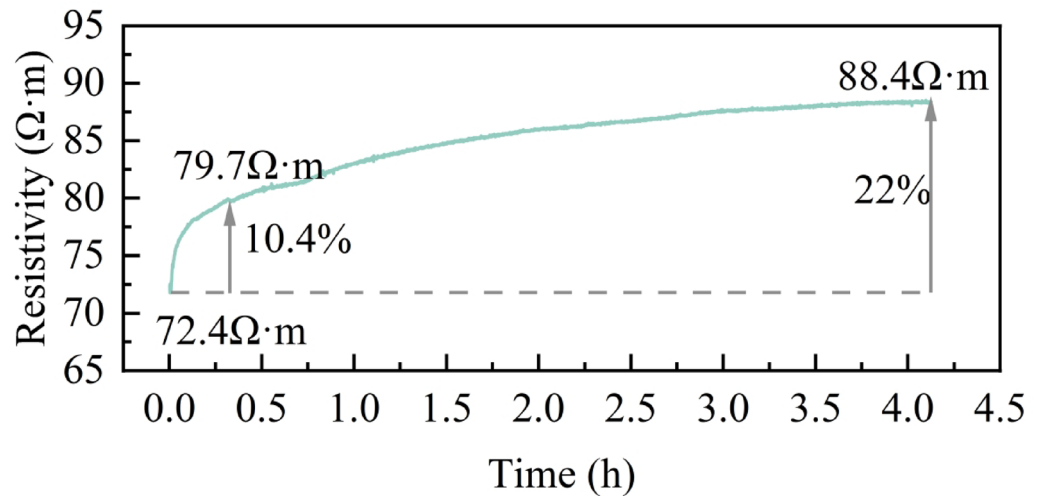


Fig. 6. Time history of equivalent resistance during electrolysis desaturation process.

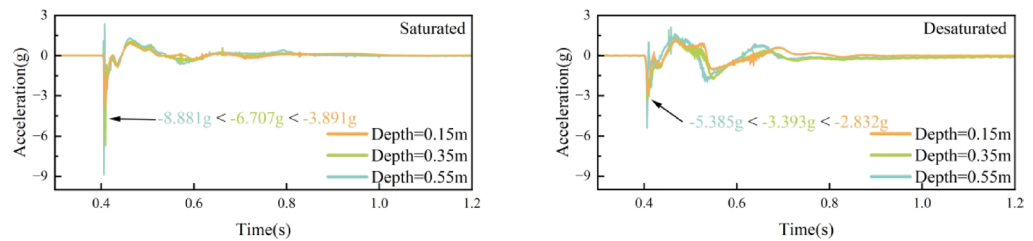


Fig. 7. Acceleration time history at different heights of the quay wall: (a) saturated condition; (b) desaturated condition.

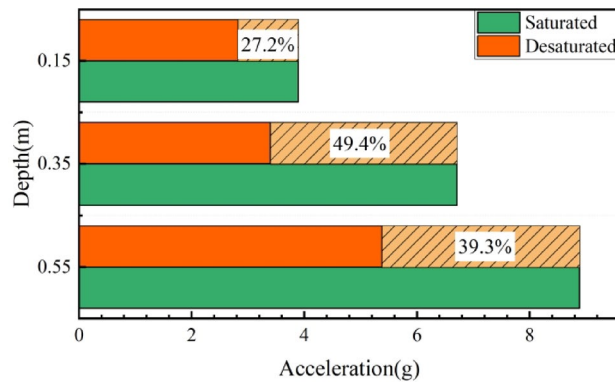


Fig. 8. Percentage reduction in peak acceleration versus depth for the quay wall.

is shown in Fig. 7. Regarding acceleration amplitude, the measurements show a consistent increase with depth regardless of desaturation treatment. In all cases, the maximum acceleration amplitude occurs at the bottom of the quay wall. This is because the distance between the bottom of the quay wall and the explosives is smaller. This is consistent with the overall trend of Ni's⁴⁶ experimental results, but due to the fact that the accelerometer in this experiment was fixed to a gravity quay wall, the integrity of the quay wall prevented the acceleration change trend with a turning point, which is different from Ni⁴⁶.

Figure 8 shows that after the desaturation treatment, the acceleration amplitude are reduced significantly, where the peak acceleration was reduced by 27–50%, indicating that after the desaturation treatment, the existence of bubbles reduced the pore fluid bulk modulus and was able to absorb more energy. And with the decrease in saturation, the matric suction of the soil skeleton increases, improving the ability of the soil to bear

loads, leading to an increase in the overall strength of the soil, resulting in a reduction in the loads on the quay wall.

Pore water pressure response

In the tests, the values of excess pore pressure during liquefaction were directly measured, then, according to the location of the pore pressure transducer and the degree of density and saturation of the soil, the vertical effective stress at the corresponding position is calculated. The excess pore pressure ratio R_u is approximately calculated as the ratio of excess pore water pressure Δu to the initial vertical effective stress σ'_{v0} before explosion, as shown in Eq. (5):

$$R_u = \frac{\Delta u}{\sigma'_{v0}} \quad (5)$$

Electrolysis desaturation treatment replaces part of the pore water in the soil with air bubbles. When an explosion wave propagates through this soil, the gas bubbles compress easily under pressure, reducing excess pore pressure buildup. As a result, the excess pore pressure time-history shows different accumulation and dissipation patterns compared to saturated soil. The time-history curves of R_u at different depths in Section 1 (Fig. 4) are illustrated in Fig. 9, revealing four distinct characteristics.

First, compared to the saturated condition, the peak R_u in desaturated soil decreases during explosion wave propagation due to the reduced pore fluid modulus. Subsequently, the excess pore pressure ratio temporarily stabilizes at a constant value (indicated by red dots in Fig. 9). The excess pore pressure ratio at this stage is termed the non-peak incremental excess pore pressure ratio. The data show that after desaturation treatment, this non-peak increment decreases but exhibits prolonged stability⁴⁷ (marked by a temporary plateau). This behavior occurs because gas bubbles can recover their original state after high-pressure explosion wave propagation ceases, extending the duration of the non-peak increment. Furthermore, as pore pressure dissipates, the reduction in soil permeability caused by lower saturation degrees substantially decreases dissipation rates. This leads to a smaller pore pressure ratio difference over comparable time periods, similar to the response observed under existing structures.³⁸ Therefore, at a certain moment, the excess pore pressure ratio under desaturated conditions is equal to the excess pore pressure ratio under saturated conditions, as marked by the green dots in Fig. 9. After this moment, the excess pore pressure ratio under desaturated conditions is higher than the excess pore pressure ratio under saturated conditions.

In previous studies, confirming soil liquefaction due to large strains and stresses induced by explosion waves^{48–50}. It should be noted that values of $R_u > 1.0$ were observed. This is because, when the explosion wave propagates to the pore pressure gauge location, both the effective stress of the soil and the excess pore water pressure increase instantaneously. Theoretically, the R_u should be calculated using the increased effective stress and excess pore water pressure at this time. However, when calculating R_u , the effective stress under static conditions is used. At this time, the effective stress under static conditions is less than the actual effective stress, so $R_u > 1$. This is a commonly used calculation method, that is also used in shake table tests.

Although the excess pore pressure ratio dissipates more slowly and maintains higher residual values in desaturated conditions compared to saturated conditions, but in the desaturation condition, the lateral displacement and tilt angle of the quay wall are smaller in the liquefaction stage (stage II), the desaturated soil remains stable without full liquefaction. Therefore, the time of full liquefaction of the soil is shorter under unsaturated conditions. Notably, when the ratio exceeds 1.0, desaturated conditions exhibit lower excess pore pressure than saturated conditions.

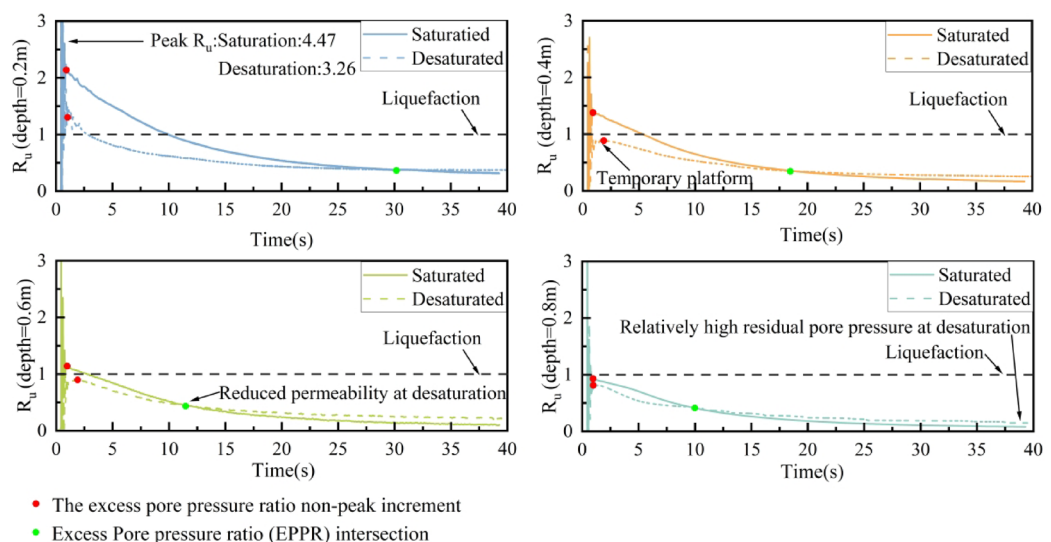


Fig. 9. Time history curves of excess pore pressure ratio at different depths on Section 1.

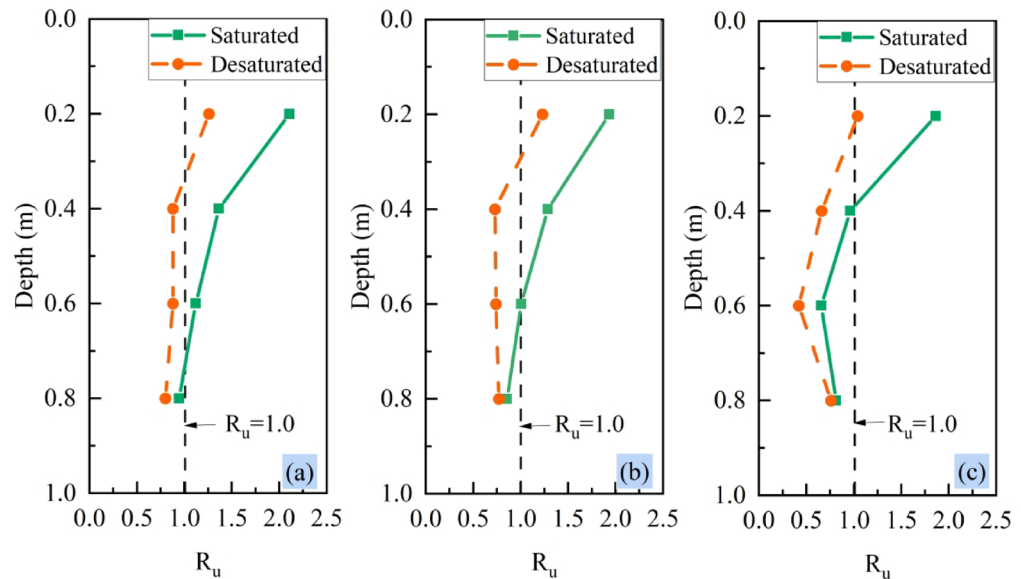


Fig. 10. Variation of EPPR along the depth direction for (a) Section 1; (b) Section 2; (c) Section 3.

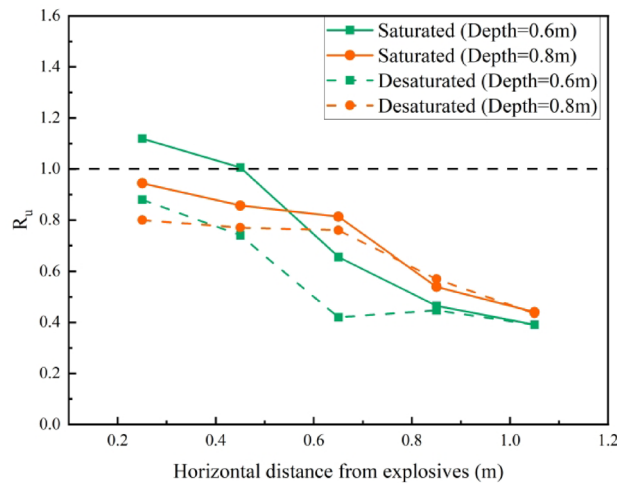


Fig. 11. Variation of deeply EPPR along the horizontal direction.

In Fig. 9, the peak excess pore pressure ratio falls outside the range of interest for liquefaction studies. Since this investigation focuses on the lateral spreading stage following explosion wave propagation, the intense fluctuations in the peak region of Fig. 9 are excluded from analysis and only the stable phase of excess pore pressure ratio variation is considered in analysis.

As shown in Fig. 9, desaturation treatment significantly reduced both the excess pore pressure ratio and the liquefaction duration (when $R_u > 1.0$) to 40–60% of saturated condition values, indicating the effectiveness of the desaturation treatment.

The non-peak incremental excess pore pressure ratio at different depths and sections are shown in Figs. 10 and 11. Figure 10 shows that the non-peak incremental excess pore pressure ratio decreases with depth. This occurs because the rate of excess pore pressure increase becomes proportionally smaller than the effective stress increase. In addition, due to the setting of an impermeable boundary, the excess pore pressure can only dissipate upwards, which also leads to an increase in the non-peak increment of excess pore pressure ratio and liquefaction duration at shallow locations. This is consistent with the fact that shallow layers have greater liquefaction potential in actual earthquakes^{51,52}.

In Figs. 10 and 11, it is shown that the excess pore pressure ratio decreases with decreasing distance from the quay wall, both horizontally in the lateral spreading soil and at the base of the quay wall. This is due to the high stiffness of the quay wall, the closer the part of the quay wall is to the dynamic action is less, so that the excess pore pressure ratio of the cross section close to the quay wall decreases.

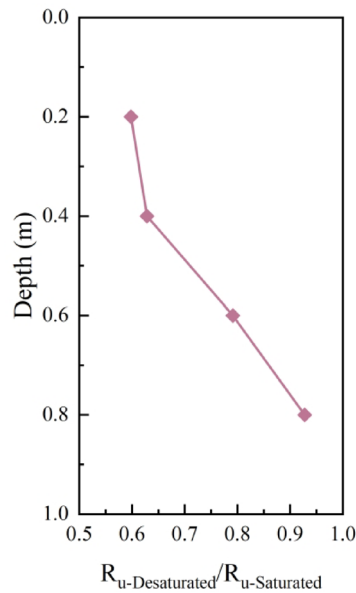


Fig. 12. Excess pore pressure ratios of desaturated to saturated sand at different depths.

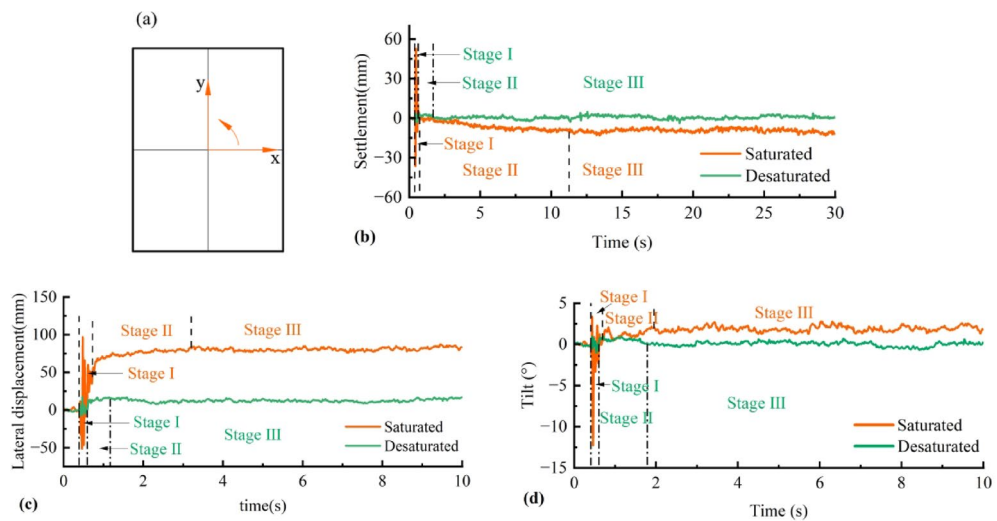


Fig. 13. Time history of displacement of the quay wall: (a) Displacement in positive direction; (b) Settlement time history; (c) Horizontal displacement time history; (d) Tilt time history.

Summarizing Figs. 10 and 11, the non-liquefied portion of the lateral spreading soil can wrap around the liquefied portion of the soil at a distance to the quay wall in the form of a bowl, creating a very small lateral displacement. Therefore, if the economic aspect is taken into account, and ensure the stability of gravity quay walls in liquefaction, reinforcement along the depth of the part of the region close to the back of the quay wall is a better option, not limited to the method of desaturation reinforcement.

Figure 12 presents the ratio of the mean excess pore pressure ratio for the desaturated condition to the mean excess pore pressure ratio for the saturated condition at different depth, with an average reduction in excess pore pressure ratio of 40% in the desaturated region.

Movement of the quay wall

Figure 13 displays the time-history of quay wall movements recorded during testing. The displacement data, collected from three sensors mounted at the top of the wall, were processed using the wall’s center as the coordinate origin, with counterclockwise tilt defined as the positive direction.

The three sets of time-history curves reveal similar movement patterns between both test groups, divisible into three distinct stages. In the first stage, when the wharf wall was subjected to the blast wave, the soil pressure on the onshore side of the wharf wall was greater than the water pressure on the offshore side. Consequently,

		Saturated		Desaturated	
		Time (s)	Value	Time (s)	Value
Settlement (mm)	End of stage I	0.73	0.857	0.635	2.587
	End of stage II	11.3	-9.88	1.169	0.778
Lateral displacement (mm)	End of stage I	0.724	46.54	0.597	1.209
	End of stage II	3.2	82	1.167	15.96
Tilt (°)	End of stage I	0.692	0.567	0.601	0.055
	End of stage II	1.950	1.985	1.782	0.131

Table 2. Displacement values at the end of each stage of the quay wall.

Damage level	Level I: repairable	Level II: operational	Level III: near collapse	Level IV: collapse
Tilt ratio (d/H)	< 1.5%	1.5–5%	5–10%	> 10%
Seaward tilt of caisson	< 3°	3–5°	5–8°	> 8°

Table 3. Proposed damage criteria for gravity quay walls. d = horizontal displacement at the top of the caisson; H = height of the caisson.

the wharf wall moved laterally a certain distance while shaking repeatedly. The blast wave was the main cause of structural displacement in this stage. In the second stage, the quay wall undergoes displacement under static conditions at a decreasing rate over time until it comes to a gradual stop⁵³. The dissipation of accumulated excess pore pressure during this stage is the primary reason for the quay wall displacement, which is the focus of this study. In the third stage, the excess pore pressure dissipates to non-liquefied levels and foundation capacity reaches the stability threshold. This results in a stabilized soil-quay wall system, representing the final equilibrium state following liquefaction-induced lateral spreading.

Table 2 has summarized the time and displacement for each stage of the quay wall movement time history. In terms of the time at the end of each stage, the time at the end of the explosion wave (stage I) and the time at which the pore water pressure dissipated (stage II) were shorter after the desaturation treatment.

The displacement comparisons demonstrate that electrolysis desaturation treatment significantly reduces quay wall movement. Most notably, lateral displacements decreased by 80.5% overall (from 82 to 15.96 mm), with the liquefaction-induced component showing a 58.4% reduction (from 35.46 to 14.75 mm). The changes in tilt and settlement of the quay wall are small relative to the absolute values of lateral displacement, where the direction of the tilt angle indicates the existence of a potential sliding surface. After the desaturation treatment, the settlement values waved around the zero point because of the limited loss of shear stiffness in the partially saturated soils and the fact that liquefaction did not occur in some areas close to the quay wall.

Discussion

The effect of desaturation on hydraulically filled foundations

The lower rate of pore pressure dissipation in the desaturated condition can be attributed to two main factors. The first and most important reason is related to fluid compressibility. In saturated soil, the pore fluid (water) is essentially incompressible, so even a small amount of drainage leads to a significant reduction in pore pressure. In desaturated soil, the pore fluid is a mixture of water and air. Due to the compressibility of air, the same amount of water drainage does not produce a comparable reduction in pore pressure, as the air bubbles can partially compensate pressure loss by increasing the air bubble volume. The second reason is that desaturated soil has lower permeability compared to saturated soil. As a result, the rate of water drainage is reduced, which further slows the dissipation of pore pressure. Together, these mechanisms explain both the slower dissipation rate and the brief stabilization plateaus.

A closer examination of the dissipation curves shows that the difference in residual pore pressure between saturated and desaturated conditions occurs only within a very short time (less than 1 min). From an engineering perspective, this duration is negligible, as in both cases the residual pore water pressure dissipates rapidly, allowing the soil to return to its initial effective stress state. Approximately 80% of the excess pore pressure is released within this brief period, indicating that the majority of effective stress is quickly regained. Consequently, the potential for observing any significant impact on reconsolidation settlement or the cyclic softening mechanism is limited. Furthermore, the differences in dissipation trends and magnitudes between saturated and desaturated sands are not substantial enough to raise concerns that desaturation introduces new issues related to residual pore pressure.

Desaturation treatment mitigates liquefaction damage to quay walls

Tables 3 and 4 present the damage criteria for gravity quay walls and performance grade based on the importance category of port structures recommended by the International Navigation Association in “Seismic Design Guidelines For Port Structures”⁵⁴. The tilt ratios calculated using saturated and desaturated conditions are 7.88% and 3.23%, respectively. Under saturated conditions, the damage level of the gravity quay wall is Level III: Near Collapse. After desaturation treatment, the damage level of the structure changes to Level II: Operational,

Performance grade	Definition based on seismic effects on structures
Grade S	① Critical structures with potential for extensive loss of human life and property upon seismic damage
	② Key structures that are required to be serviceable for recovery from earthquake disaster
	③ Critical structures that handle hazardous materials
	④ Critical structures that, if disrupted, devastate economic and social activities in the earthquake damage area
Grade A	Primary structures having less serious effects for ① through ④ than Grade S structures, or ③ Structures that, if damaged, are difficult to restore
Grade B	Ordinary structures other than those of Grades S, A and C
Grade C	Small easily restorable structures

Table 4. Performance grade based on the importance category of port structures.

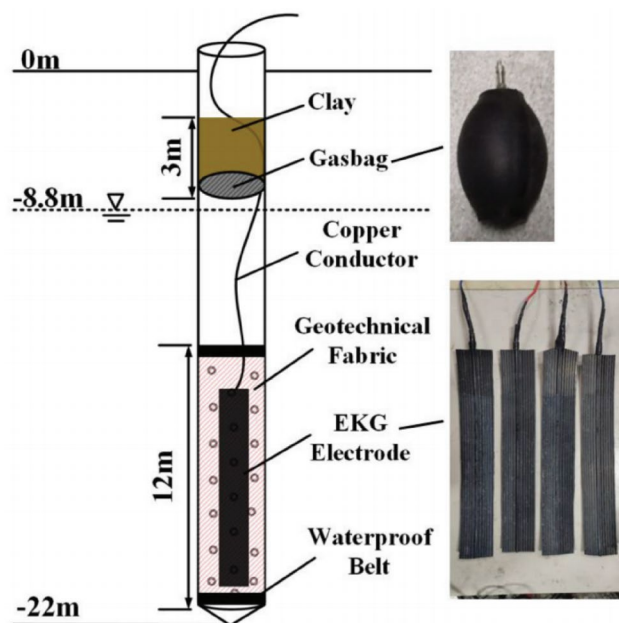


Fig. 14. Schematic of electrode arrangement method⁵⁵.

thereby mitigating the damage caused by liquefaction to the gravity quay wall and playing a certain role in reducing losses to people and economic property.

Although the tilt ratios in Tables 3 and 4 are scale-independent, the absolute horizontal displacements they represent in a prototype quay wall are an order of magnitude larger; consequently, the same percentage tilt may exceed port serviceability tolerances in the field even though it is tolerable in the model.

Practical field implementation challenges

Electrolytic desaturation faces several challenges during actual field implementation. The first challenge is the deep electrode placement. In this study, the horizontal electrode arrangement was adopted, because it was considered that during the hydraulic filling process, the electrodes could be placed at the required position below the water surface before filling behind the quay wall, which is consistent with the process of this experiment. For in-situ sand below the hydraulic fill depth, the higher density and cementation properties reduce the potential of liquefaction. If it is necessary to treat deep in-situ sand, we can drill boreholes to install electrodes or employ electrolysis piles equipped with electrodes.

Second is electrode corrosion under saline-alkali conditions. The electrode material adopted in this study is graphite felt, which is made of polyacrylonitrile and possesses excellent conductivity. It is used in the chemical industry as a high-purity filtration material for corrosive chemical reagents. Another type is conductive plastic, which is made by adding conductive materials (such as Ketjen Black carbon or carbon fiber) to an insulating base material (Thermoplastic Polyurethane) to achieve electrical conductivity. Examples are EKG electrode⁵⁵, as shown in Fig. 14. The majority of the conductive elements in these materials are carbon rather than metals, thus there is no risk of electrode corrosion.

Next is the power supply guarantee. In this test, the electrolysis current was maintained at 1 A, with the voltage increasing from 10.8 to 13.2 V, the power supply capacity is 13.2 W. Using the same current density and according to the deep-water port requirement of -15 m water depth, the corresponding similarity ratio can be approximated as 1:30. For a 45 m wide and 16.5 m deep berth, the required power is approximately 72 kW. According to research by some scholars, the pore water behind the quay wall remains stationary year-round, and

gases have good stability under static water conditions. To ensure the effectiveness of liquefaction mitigation, electrolysis can be conducted once per week for 4 h per treatment. The required power capacity is 288 kW h/week. When employing sequential electrolysis of the electrolytic region, the power consumption is 1.7 kW. This is equivalent to the power consumption of an air conditioner, which is negligible for port facilities. Therefore, insufficient power supply is not a consideration.

Conclusion

Field blast-induced liquefaction tests were conducted to study the effectiveness of desaturation treatment of gravity quay walls during liquefaction of laterally spreading sites. From this study, the following conclusions can be drawn.

1. Field blast tests show that a modest reduction in saturation ($\approx 20\%$) shortens liquefaction duration by 30–50% and cuts the free-field excess pore-pressure ratio by 40%. For a gravity caisson this translates into a one-class reduction in damage level (III \rightarrow II) and an 80% decrease in lateral spreading, confirming that electrolytic desaturation can be used as a life-cycle liquefaction countermeasure for existing and new quay walls on coral-sand islands.
2. The treatment is compatible with ordinary port construction plant: perforated graphite-felt anodes/cathodes are laid horizontally during hydraulic filling and are connected to a low-voltage DC source (1.48 A m⁻² electrode area). Four hours of power input raised the electrode resistance by 22% and lowered saturation from 100 to 81% in the 0.9 m \times 0.75 m treatment zone; the same energy density is expected to produce a similar saturation drop in thicker deposits because bubble generation is governed by current density, not total thickness.
3. Because gas bubbles increase pore-fluid compressibility without reducing soil stiffness, the method preserves the in-service settlement performance of the fill while improving its seismic margin. This avoids the post-treatment rebound and re-consolidation settlements that often follow densification or drainage-based ground improvement.
4. Electrode spacing, treatment duration and power demand scale linearly with the volume of sand to be desaturated. For a 45 m-wide berth built on 15 m of hydraulically filled coral sand, a treatment using 1.7 kW electrical power and reusable graphite-felt electrodes is estimated to cost < 3% of the caisson super-structure and can be carried out between dredging phases, making the technique economically attractive for large-scale reclamations in the South China Sea and similar carbonate-rich environments.

Limitations of the study

This study has certain limitations. First, there are differences between the reconstituted sand samples and the undisturbed sand samples. Second, the results of the explosion tests have a certain degree of randomness, and the reproducibility of the tests is poor. Additionally, most existing tests have not considered the variability of large-scale foundations. Despite attempts to control the accuracy of the tests, due to the above factors, errors in the test results are inevitable.

Additionally, we fully acknowledge that the blast loading used in this study to evaluate the liquefaction behavior of the foundation cannot reproduce all earthquake characteristics, such as long-duration shaking or low-frequency resonance effects. Therefore, the results should not be interpreted in terms of dynamic response spectra or soil–structure resonance. Instead, the findings are most applicable to liquefaction triggering, pore-pressure generation, and quay wall movement patterns, which remain reliable under the adopted loading method.

Therefore, this study is only a test conducted under specific conditions. In order to conduct more accurate research and discussion on the liquefaction characteristics of desaturated samples, it is necessary to carry out experimental studies such as dynamic triaxial tests and hollow cylindrical shear tests.

Data availability

The datasets used and/or analyzed during the current study available from the corresponding author on reasonable request.

Received: 23 May 2025; Accepted: 17 October 2025

Published online: 21 November 2025

References

1. Lv, C., Wu, H., Shi, M. & Zhang, D. Experimental study on the mechanical strength, deformation behavior and infiltration characteristics of coral sand. *Sustainability* **16**, 3479 (2024).
2. Shahnazari, H., Jafarian, Y., Tutunchian, M. A. & Rezvani, R. Undrained cyclic and monotonic behavior of hormuz calcareous sand using hollow cylinder simple shear tests. *Int. J. Civil Eng.* **14**, 209–219 (2016).
3. Hayakawa, K., Matsui, T. & Harada, K. *Seismic Ground Settlement and Microtremore Property in Reclaimed Lands Due to the 1995 Kobe Earthquake 2*, 558–563 (SEATTLE, WA, 2000).
4. Shahnazari, H., Jafarian, Y., Tutunchian, M. A. & Rezvani, R. Probabilistic assessment of liquefaction occurrence in calcareous fill materials of Kawaihae harbour, Hawaii. *Int. J. Geomech.* **16**, 05016001 (2016).
5. Hamada, M., Towhata, I., Yasuda, S. & Ioyama, R. Study on permanent ground displacement induced by seismic liquefaction. *Comput. Geotech.* **4**, 197–220 (1987).
6. Verdugo, R. & González, J. Liquefaction-induced ground damages during the 2010 Chile earthquake. *Soil Dyn. Earthq. Eng.* **79**, 280–295 (2015).
7. Cubrinovski, M. & Robinson, K. Lateral spreading: Evidence and interpretation from the 2010–2011 Christchurch earthquakes. *Soil Dyn. Earthq. Eng.* **91**, 187–201 (2016).

8. Kiyota, T., Furuichi, H., Hidayat, R. F., Tada, N. & Nawir, H. Overview of long-distance flow-slide caused by the 2018 Sulawesi earthquake, Indonesia. *Soils Found.* **60**, 722–735 (2020).
9. Zhang, Y., Ding, X., Chen, Z., Wu, Q. & Wang, C. Seismic responses of slopes with different angles in coral sand. *J. Mt. Sci.* **18**, 2475–2485 (2021).
10. Dakoulas, P., Vazouras, P., Kallioglou, P. & Gazetas, G. Effective-stress seismic analysis of a gravity multi-block quay wall. *Soil Dyn. Earthq. Eng.* **115**, 378–393 (2018).
11. Hwang, G.-S. & Chen, C.-H. Analysis of cases of gravity quaywall movement during earthquakes. *Geotechnique* **61**, 199–210 (2011).
12. Han, S., Gong, J. & Zhang, Y. Seismic sliding and rotational displacement of gravitational retaining structures with saturated backfill sand. *Chin. J. Rock Mech. Eng.* **35**, 162–176 (2016).
13. Liu, W. Effect analysis of vacuum prepressing reinforcement of soft soil foundation. In *IOP Conference Series-Earth and Environmental Science* 358, 042040 (IOP Publishing, 2019).
14. Zhou, Y. et al. Experimental and consolidation modeling of flowing mud during vacuum preloading considering transient clogging and vacuum pressure attenuation. *Geotext. Geomembr.* **53**, 767–779 (2025).
15. Krishnapriya, P. B., Sandeep, M. N. & Antony, J. Efficiency of vacuum preloading on consolidation behaviour of Cochin marine clay. In *Procedia Technology* 24, 256–262 (Trichur, India, 2016).
16. Xu, G., Liu, Y., Ni, J., Cao, Y. & Deng, S. Influence of soil crack on large-deformation consolidation of dredged clay under vacuum preloading: A numerical solution. *Comput. Geotech.* **183**, 107161 (2025).
17. Wang, J. et al. Improved vacuum preloading method for consolidation of dredged clay-slurry fill. *J. Geotech. Geoenviron. Eng.* **142**, 06016012 (2016).
18. Zhang, Z., Ye, G.-B. & Xu, Y. Comparative analysis on performance of vertical drain improved clay deposit under vacuum or surcharge loading. *Geotext. Geomembr.* **46**, 146–154 (2018).
19. Wang, J. et al. Secondary compression behavior of over-consolidated soft clay after surcharge preloading. *Acta Geotech.* **17**, 1009–1016 (2022).
20. Yao, Y.-X. & Ji, F.-Y. Analysis of monitoring in settlement for vacuum combined stack preloading about soft foundation sluice. *IOP Conf. Ser. Earth Environ. Sci.* **446**, 052067 (2020).
21. Hu, X., Zhang, W. & Wang, J. Experimental study on dynamic compaction to improve saturated soft clay covered with hydraulic fill sand. *Rock Soil Mech.* **25**, 817–823 (2004).
22. Sun, J., Ge, X. & Li, P. Vibration mechanism and energy transfer analysis of dynamic compaction method on ground with high groundwater level. *Int. J. Geomech.* **23**, 04023200 (2023).
23. Wei, J., Men, Y., Zhu, F., Le, H. & Fan, H. The reinforcement effects of deep soft soil foundation with high degree of saturation under dynamic compaction. *Adv. Mech. Eng.* **10**, 1687814018782633 (2018).
24. Okamura, M., Ishihara, M. & Tamura, K. Degree of saturation and liquefaction resistances of sand improved with sand compaction pile. *J. Geotech. Geoenviron. Eng.* **132**, 258–264 (2006).
25. He, H., Lin, Y., Li, J. & Zhang, N. Immersed tunnel foundation on marine clay improved by sand compaction piles. *Mar. Georesour. Geotechnol.* **36**, 218–226 (2018).
26. Yabe, H., Takeuchi, H., Ogata, F. & Harada, K. Sand compaction pile method utilizing recycled materials. In *Sustainable Construction Resources in Geotechnical Engineering* (eds Hazarika, H., Haigh, S. K., Chaudhary, B., Murai, M. & Manandhar, S.) 267–280 (Springer, Singapore, 2024).
27. Padmanabhan, G. & Shanmugam, G. K. Liquefaction and reliquefaction resistance of saturated sand deposits treated with sand compaction piles. *Bull. Earthq. Eng.* **19**, 4235–4259 (2021).
28. Li, Y., Kitazume, M., Takahashi, A. & Harada, K. Effect of SCP improvement geometry on mitigation of liquefaction-induced embankment settlement. In *Geotechnics for Sustainable Infrastructure Development* (eds Duc Long, P. & Dung, N. T.) 62, 657–664 (Springer, Singapore, 2020).
29. Kuerban, F., Li, H., Peng, Y., Zhou, Y. & Wang, Y. Experimental study on the treatment effect of vibroflotation gravel piles for saturated sand foundations in coastal areas. *Arab. J. Sci. Eng.* **47**, 4833–4848 (2022).
30. Sugianto, A., Tamsir, P. C. & Rahardjo, P. P. Sand densification using combination of vibroflotation and stone column for coastal reclamation in Lampung, Indonesia. In *Geotechnics for Sustainable Infrastructure Development* (eds Duc Long, P. & Dung, N. T.) 62, 1359–1366 (Springer, Singapore, 2020).
31. O'Donnell, S. T., Rittmann, B. E. & Kavazanjian, E. MIDP: Liquefaction mitigation via microbial denitrification as a two-stage process. I: desaturation. *J. Geotech. Geoenviron. Eng.* **143**, 04017094 (2017).
32. Peng, E., Zhang, D., Sun, W. & Du, G. Desaturation for liquefaction mitigation using biogas produced by *Pseudomonas stutzeri*. *J. Test. Eval.* **46**, 20170435 (2018).
33. Wang, L. et al. Laboratory tests on mitigation of soil liquefaction using microbial induced desaturation and precipitation. *Geotech. Test. J.* **44**, 520 (2020).
34. Hall, C. A., Van Paassen, L. A., Kamalzare, S., Parmantier, D. & Kavazanjian, E. Techno-economic assessment of liquefaction mitigation by microbially induced desaturation. In *Lifelines 2022* 91–100 (American Society of Civil Engineers, Virtual Conference, 2022). <https://doi.org/10.1061/9780784484449.008>
35. Okamura, M. Full scale test on cost effective liquefaction countermeasure for highway embankment. *J. Seismol. Res.* **40**, 45–51 (2017).
36. Sorenson, K. et al. Field monitoring of the persistence of microbially induced desaturation for mitigation of earthquake induced soil liquefaction in silty soil. In *Lifelines 2022* 101–113 (American Society of Civil Engineers, Virtual Conference, 2022). <https://doi.org/10.1061/9780784484449.009>
37. He, J., Chu, J., Wu, S. & Peng, J. Mitigation of soil liquefaction using microbially induced desaturation. *J. Zhejiang Univ. Sci. A* **17**, 577–588 (2016).
38. Lv, M., Zhang, D. & Xu, T. Seismic response of mitigation of sand liquefaction beneath existing buildings using microbial induced desaturation. *Case Stud. Constr. Mater.* **20**, e02926 (2024).
39. Karmacharya, D. A *Large-Scale Experiment on Performance of MIDP in Stratified Silty Sand* (Arizona State University, Tempe, 2023).
40. Zhang, Z., Chen, Y., Liu, H., Zhou, Y. & Zhou, X. Resistivity characteristics during horizontal-layered electrolysis desaturation of calcareous sand. *Eng. Geol.* **279**, 105899 (2020).
41. Chen, Y., Zhou, Y., Chen, R., Sarajpoo, S. & Xie, X. Electrical characteristics and desaturation effectiveness during horizontal electrolysis in calcareous sand. *Buildings* **15**, 2061 (2025).
42. Zhongyue, R., Shichun, Z. & Yumin, C. Liquefaction characteristics of desaturated coral sand foundation with upper building. *Sci. Rep.* **15**, 17006 (2025).
43. D18 Committee. Practice for classification of soils for engineering purposes (Unified Soil Classification System). <https://doi.org/10.1520/D2487-11>
44. Dong, Q., Wei, Z., Tang, T., Li, L. & Liu, J. Damage effects of caisson gravity wharf under underwater explosion. *Explos. Shock Waves* **39**, 113–123 (2019).
45. Keller, G. V. & Frischknecht, F. C. *Electrical Methods in Geophysical Prospecting* (Pergamon Press, 1966).
46. Ni, S. et al. Blast liquefaction test of saturated sand foundations disposed by a drainage rigid pile. *Shock. Vib.* **2022**, 1–18 (2022).

47. Baziar, M. H., Khoshniazpirkoohi, A. & Amirabadi, O. E. Mitigation of liquefaction and lateral spreading by biogas method using shaking table tests and the strain energy approach. *Int. J. Geomech.* **22**, 04022236 (2022).
48. Koutsourelakis, S., Prévost, J. H. & Deodatis, G. Risk assessment of an interacting structure–soil system due to liquefaction. *Earthq. Eng. Struct. Dyn.* **31**, 851–879 (2002).
49. Montoya-Noguera, S. & Lopez-Caballero, F. Effect of coupling excess pore pressure and deformation on nonlinear seismic soil response. *Acta Geotech.* **11**, 191–207 (2016).
50. López Jiménez, G. A., Dias, D. & Jenck, O. Effect of the soil–pile–structure interaction in seismic analysis: Case of liquefiable soils. *Acta Geotech.* **14**, 1509–1525 (2019).
51. Zou, Y.-X., Zhang, J.-M. & Wang, R. Seismic analysis of stone column improved liquefiable ground using a plasticity model for coarse-grained soil. *Comput. Geotech.* **125**, 103690 (2020).
52. Zhuang, H. et al. Seismic responses of a subway station and tunnel in a slightly inclined liquefiable ground through shaking table test. *Soil Dyn. Earthq. Eng.* **116**, 371–385 (2019).
53. Zeybek, A. & Madabhushi, S. P. G. Influence of air injection on the liquefaction-induced deformation mechanisms beneath shallow foundations. *Soil Dyn. Earthq. Eng.* **97**, 266–276 (2017).
54. International Navigation Association. *Seismic Design Guidelines For Port Structures* (Balkema Publishers, 2001).
55. Chen, R. et al. In situ desaturation tests by electrolysis for liquefaction mitigation. *Can. Geotech. J.* **58**, 1744–1756 (2021).

Author contributions

Junwei Guo: Conduct field tests and wrote the main manuscript. Yumin Chen: Provide guidance for field tests and paper writing. Xiao Xie: Conducting field test. Yingkang Yao: Conducting field test and provide guidance for paper writing. Changchun Li: Revision of the English version of the main manuscript. Qiongtong Wang: Conducting field test.

Funding

This work was supported by the National Natural Science Foundation of China (Grant no. 52179101) and the State Key Laboratory of Precision Blasting and Hubei Key Laboratory of Blasting Engineering, Jianghan University (Grant no. PBSKL2022B02).

Declarations

Competing interests

The authors declare no competing interests.

Additional information

Correspondence and requests for materials should be addressed to Y.C.

Reprints and permissions information is available at www.nature.com/reprints.

Publisher's note Springer Nature remains neutral with regard to jurisdictional claims in published maps and institutional affiliations.

Open Access This article is licensed under a Creative Commons Attribution-NonCommercial-NoDerivatives 4.0 International License, which permits any non-commercial use, sharing, distribution and reproduction in any medium or format, as long as you give appropriate credit to the original author(s) and the source, provide a link to the Creative Commons licence, and indicate if you modified the licensed material. You do not have permission under this licence to share adapted material derived from this article or parts of it. The images or other third party material in this article are included in the article's Creative Commons licence, unless indicated otherwise in a credit line to the material. If material is not included in the article's Creative Commons licence and your intended use is not permitted by statutory regulation or exceeds the permitted use, you will need to obtain permission directly from the copyright holder. To view a copy of this licence, visit <http://creativecommons.org/licenses/by-nc-nd/4.0/>.

© The Author(s) 2025